

Shifts in water supply and demand shape land cover change across Chile¹

Francisco Zambrano^{a,b}, Anton Vrieling^c, Francisco Meza^{d,e,f}, Iongel Duran-Llacer^g, Francisco Fernández^{b,h,i}, Alejandro Venegas-González^{b,j}, Nicolas Raab^d, and Dylan Craven^{b,k,l}

^a Hémera Centro de Observación de la Tierra, Facultad de Ciencias, Escuela de Ingeniería en Medio Ambiente y Sustentabilidad, Universidad Mayor, Santiago, Chile.

^b Observatorio de Sequía para la Agricultura y la Biodiversidad de Chile (ODES), Universidad Mayor, Santiago, Chile.

^c Faculty of Geo-Information Science and Earth Observation (ITC), University of Twente, Enschede, The Netherlands.

^d Facultad de Agronomía y Sistemas Naturales, Pontificia Universidad Católica de Chile., Santiago, Chile.

^e Instituto para el Desarrollo Sustentable. Pontificia Universidad Católica de Chile, Santiago, Chile.

^f Centro Interdisciplinario de Cambio Global, Pontificia Universidad Católica de Chile, Santiago, Chile.

^g Hémera Centro de Observación de la Tierra, Facultad de Ciencias, Universidad Mayor, Santiago, Chile.

^h Center of Economics for Sustainable Development (CEDES), Faculty of Economics and Government, Universidad San Sebastián, Santiago, Chile.

ⁱ Center of Applied Ecology and Sustainability (CAPES), Santiago, Chile.

^j Instituto de Ciencias Agroalimentarias, Animales y Ambientales (ICA3), Universidad de O'Higgins, San Fernando, Chile.

^k GEMA Center for Genomics, Ecology & Environment, Universidad Mayor, Camino La Pirámide Huechuraba 5750, Santiago, Chile.

^l Data Observatory Foundation, Santiago, Chile.

Corresponding author. Email: francisco.zambrano@umayor.cl; dylan.craven@umayor.cl

Abstract

Globally, droughts are becoming longer, more frequent, and more severe, and their impacts are multidimensional. These impacts typically extend beyond the water balance, as long-term, cumulative changes in the water balance can lead to regime shifts in land cover. Here, we assess the effects of temporal changes in water supply and demand over multiple time scales on vegetation productivity and land cover changes in continental Chile, which has experienced a severe drought since 2010. Across most of continental Chile, we observed a persistent negative trend in water supply and a positive trend in atmospheric water demand since 2000. However, in water-limited ecoregions, we have observed a negative temporal trend in the water demand of vegetation, which intensified over longer time scales. This long-term decrease in water availability and the shift in water demand have led to a decrease in vegetation productivity, especially for the Chilean Matorral and the Valdivian temperate forest ecoregions. We found that this decrease is primarily associated with drought indices associated with soil moisture and actual evapotranspiration at time scales of up to 12 months. Further, our results indicate that drought intensity explains up to 78% of temporal changes in the area of shrublands and 40% of the area of forests across all ecoregions, while the burned area explained 70% of the temporal changes in the area of croplands. Our results suggest that the impacts of long-term climate change on ecosystems

¹ This paper is a non-peer reviewed preprint submitted to EarthArXiv.

will extend to drought-tolerant vegetation types, necessitating the development of context-specific adaptation strategies for agriculture, biodiversity conservation and natural resource management.

Introduction

Across many regions of the world, droughts are becoming longer, more frequent, and more severe^{1,2}, impacting ecosystems *via* tree mortality³, reducing vegetation productivity¹ and inducing shifts in land use and cover⁴. However, identifying drought events is idiosyncratic due to the varying criteria used for classification. Droughts can be classified as 1) meteorological, i.e., when precipitation in a specific period falls below mean precipitation values observed over multiple years⁵ (usually more than 30 years); 2) hydrological, i.e., when precipitation anomalies last for long periods (months to years) and affect the hydrological system^{6,7} (e.g., streamflows, reservoirs and groundwater); 3) agricultural, i.e. when precipitation deficits negatively impact plant health, leading to decreases in crop or pasture productivity⁸; or 4) ecological, i.e., when water availability negatively affect the provisioning of ecosystem services and trigger feedbacks in natural or human systems⁴. Such feedbacks include drought impacts on human decision making and activities, which can lead to land-cover change^{9,10}, which may have cascading effects on biodiversity and ecosystem services (e.g., ref. 11, 12). Despite the high degree of confidence in the impacts of rising temperatures on the extent, frequency, and severity of agricultural and ecological droughts², which are likely to increase even if global warming stabilizes at 1.5°–2°C, the severity of meteorological droughts has been remarkably stable globally over the past century^{13,14}. A global study analyzing drought severity trends from 1980 to 2020 reveals that in a few regions (some mid-latitudinal and subtropical areas), rising temperatures during the warm season have increased atmospheric evaporative demand (AED), leading to an increase in agricultural land area¹³. Thus, rising water demand may reflect parallel changes in land cover—primarily agriculture—that can exacerbate the effects of meteorological droughts on ecosystems.

Expanding analyses to include multiple dimensions of droughts can provide complementary insights into the Earth's water balance - and its impacts - over multiple time scales. Yet, the World Meteorological Organization recommends the use of a single drought index for monitoring droughts¹⁵, i.e., the multi-scale Standardized Precipitation Index (SPI; ref. 16), which is limited in that it only considers water supply in the form of precipitation. The Standardized Precipitation Evapotranspiration Index (SPEI; ref. 17) builds upon SPI by incorporating the effects of temperature on drought, and is now used widely for drought monitoring (e.g., ref. 18, 19). Indices derived from soil moisture products^{20,21}, such as the Standardized Soil Moisture Index (SSI; ref. 22, 23) also monitor water supply and are thought to better capture water availability for crops, thus providing more relevant information for evaluating agricultural droughts. To disentangle the effects of precipitation from those of temperature¹⁷, as well as to capture droughts in terms of water atmospheric demand, AED has been integrated into the Evaporative Demand Drought Index (EDDI; ref. 24), which is particularly effective at detecting the rapid onset or intensification of droughts. To quantify vegetation water demand, one can use the actual evapotranspiration, or the amount of water removed from a surface by evaporation and

transpiration; the Standardized Evapotranspiration Index (SETI; ref. 25) can be used for this purpose. In turn, ecological droughts, which capture the joint effects of precipitation and temperature in modifying natural and productive ecosystems²⁶⁻²⁸, are complex to measure and can therefore be monitored using multiple drought indices that capture the multiple dimensions of drought, e.g., precipitation, temperature, evapotranspiration, and AED. Although such an approach accounts for the joint effects of changes in natural and productive ecosystems, its potential impacts on land cover change have been largely unexplored^{29,30}.

From 1960 to 2019, land-use change has impacted approximately one-third of the Earth's surface, which is four times more than previously thought³¹. Despite the considerable interest in land-use change dynamics (e.g. ref. 31, 32), the direction and magnitude of drought impacts on land cover change and vegetation productivity remain uncertain³³⁻³⁵. Meteorological droughts are responsible for approximately 37% of land cover change and variability in vegetation productivity globally³⁵. However, the evidence supporting these results is derived from only one drought index, SPEI, which combines a proxy for water supply - precipitation - with a proxy for water demand - AED - at one time scale (12 months). The use of only one time scale may bias results of drought impacts towards ecosystems dominated by plant growth forms such as grasses and herbs that respond more rapidly to drought stress (< 12 months). This is because physiological differences among and within dominant plant growth forms may increase (or decrease) tolerance of drought stress^{36,37}. For example, trees growing in more arid ecosystems typically respond over longer time scales than those in more humid ecosystems³⁸. Another source of uncertainty regarding drought impacts on land cover change and vegetation productivity are extrinsic factors, such as large-scale public policy (e.g., national and international reforestation initiatives), agricultural practices (e.g., clearing forest for soybean or oil palm), and rural and urban land use planning³⁹.

To deepen current knowledge on the multidimensional impacts of drought on the temporal dynamics of natural and productive ecosystems, we evaluate temporal changes in water supply and demand, net primary productivity, and land-cover change across terrestrial ecosystems in continental Chile for 2000-2023. Chile's diverse climate and ecosystems^{40,41} make it an ideal natural laboratory for assessing the dynamic interactions between climate and ecosystems, and potential impacts on land-cover change. Additionally, large parts of Chile have experienced severe drought conditions that have significantly affected vegetation and water storage in recent years; north-central Chile has faced a persistent precipitation deficit (or "mega-drought") since 2010⁴², which has broadly impacted native forests (e.g., ref. 43-45) and agricultural productivity (e.g., ref. 46-48). However, the effects of this prolonged extreme drought may also extend to changes in land cover, altering the provision of key ecosystem services and agricultural production. Here, we aim to assess: short- to long-term time trends (1 to 36 months) in multi-scalar drought indices that capture variation in the components of water balance, i.e., water supply (SPI, SPEI, SSI) and demand (EDDI, SETI) and their impacts on vegetation productivity and land cover change across continental Chile. We expect that drought intensity - independent of time scale - will decrease vegetation productivity, and that the magnitude of these impacts will be stronger for drought indices associated with soil moisture (i.e., SSI) and evapotranspiration (i.e.,

SETI). We further assess the relative influence of drought intensity at multiple temporal scales on land cover change, relative to human activity that may indirectly influence water demand, across ecoregions that experience droughts of varying intensity and duration. We expect that land cover change will be determined to a greater extent by drought indices at shorter time scales for land cover types dominated by vegetation with low drought tolerance, i.e., grasslands, while land cover change of more drought tolerant vegetation, i.e., forests and shrublands, will respond over longer time scales. Our integrative approach to assessing drought impacts, which combines multiple dimensions of drought (e.g., water supply and demand) across various temporal scales and its impacts (e.g., vegetation productivity and land cover change), will enhance our understanding of drought-induced ecosystem changes across different regions of the world.

Materials and Methods

Study area

Continental Chile has a diverse climate, with strong environmental gradients from north to south and east to west⁴⁹ (Fig. 1a), which, together with its complex topography (Fig. 1b), determine its ecosystem diversity^{41,50} (Fig. 1c). We therefore divided Chile into ecoregions⁵¹, which are regions that share similar geography and ecology, and have comparable levels of precipitation and solar radiation. There are seven ecoregions: Atacama desert, Central Andean dry puna, Southern Andean steppe, Chilean Matorral, Valdivian temperate forests, Magellanic subpolar forests, and Patagonian steppe. The Atacama desert is predominantly arid with hot (Bwh in the Koppen-Geiger classification) and cold (Bwk) temperatures, as well as the northern part of the Chilean Matorral. Most of the land in these two northern regions is bare, except for a small area where shrublands and grasslands are present. With an annual rainfall of less than 400 mm, the Central Andean dry puna ecoregion has low, yet highly seasonal precipitation with an eight-month dry season, low temperatures (Bwk) and is dominated by grasslands, shrublands, and savanna. The climate of the Southern Andean steppe ecoregion is cold desert (BWk), with most precipitation occurring in the winter. There is little vegetation in this ecoregion because the plants have adapted to its windy, dry, and cold climate. In central Chile, the climate of the Chilean Matorral changes to that of an arid steppe with cold temperatures (Bsk). Then, towards the center-south of the country, the climate of the Chilean Matorral changes to a Mediterranean climate, with warm to hot summers (Csa and Csb). Land cover in this ecoregion consists of a significant amount of shrublands and savannas. The Valdivian temperate forests have a mostly oceanic climate (Cfb) and a large area of forests and grasslands. The Magellanic subpolar forests have a tundra climate. Lastly, the Patagonian steppe has high aridity, cold temperatures (Bsk), and primarily consists of grasslands.

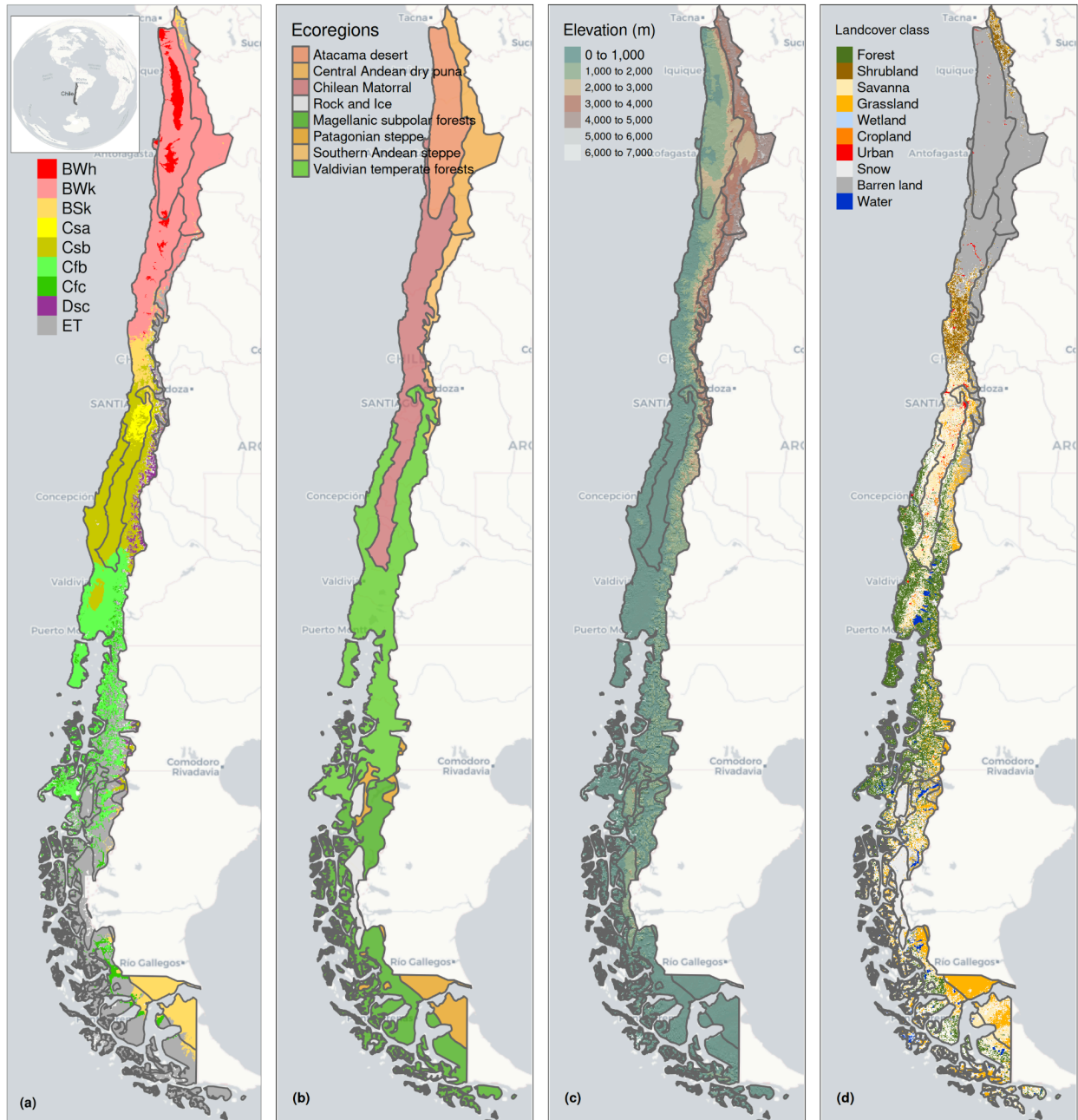


Figure 1. Climate, topography, and land cover classes across continental Chile. Koppen-Geiger climate classes (a), ecoregions (b), topography (c), and persistent land cover classes (> 80%) for 2001-2023 (d) across continental Chile.

Data

Gridded meteorological and vegetation data

To derive a proxy for vegetation productivity, we used the Normalized Difference Vegetation Index (NDVI) from the MOD13A3 Collection 6.1 product derived from the MODIS (Moderate-Resolution Imaging Spectroradiometer) sensor onboard the Terra satellite.

MOD13A3 provides vegetation indices with a 1 km spatial resolution and monthly frequency⁵². We also utilized the MOD16A2 collection 6.1⁵³ product from MODIS to gauge the water consumption of vegetation. This product gives us monthly actual evapotranspiration (ET) with a ~500m spatial resolution. For soil moisture, water supply, and water demand variables, we used ERA5-Land (ERA5L; ECMWF Reanalysis version 5 over land)⁵⁴, a reanalysis dataset that provides atmospheric and land variables since 1950. It has a spatial resolution of 0.1° (9 km), hourly frequency, and global coverage. We selected total precipitation, maximum and minimum temperature at 2 meters, and volumetric soil water layers between 0 and 100 cm of depth (layer 1 to layer 3; Supplementary Materials and Methods, Supplementary Table S2).

Gridded indicators for land use

To account for the impacts of human activity on land cover change, we obtained data on road density⁵³ and nighttime light emissions for the period 2012–2023⁵⁶. These products are frequently used in the literature to quantify the human footprint (e.g., ref. 57,58) or biodiversity threats (e.g., ref. 59, 60). To capture changes on land cover due to fires, we calculated the total burned area for 2002-2023⁶¹. For nighttime light emissions, we calculated the average annual nighttime light emissions.

Short- to long-term drought trends

Atmospheric Evaporative Demand (AED)

To compute drought indices that quantify water demand, we first calculate atmospheric evaporative demand (AED) using the Hargreaves method^{62,63}:

$$AED = 0.0023 \cdot Ra \cdot (T + 17.8) \cdot (T_{max} - T_{min})^{0.5}, (1)$$

where Ra ($MJm^2 day^{-1}$) is extraterrestrial radiation; T , T_{max} , and T_{min} are mean, maximum, and minimum temperature ($^{\circ}C$) at 2 m. For calculating Ra we used the coordinate of the latitude of the centroid of each pixel as follows:

$$R_a = \frac{14,400}{\pi} \cdot G_{sc} \cdot d_r [\omega_s \cdot \sin(\phi) \cdot \sin(\delta) + \cos(\phi) \cdot \cos(\delta) \cdot \sin(\omega_s)] (2),$$

where

Ra : extraterrestrial radiation ($MJm^{-2} day^{-1}$),

G_{sc} : solar constant = 0.0820 ($MJm^{-2} min^{-1}$),

d_r : inverse relative distance Earth-Sun,

ω_s sunset hour angle (rad),

ϕ : latitude (rad), and

δ : solar declination (rad).

We selected the method of Hargreaves to estimate AED because of its simplicity, as it only requires temperature and extraterrestrial radiation, and because access to the data needed for alternative methods (e.g., Penman-Monteith), which is often limited in Chile³⁶.

Drought indices

To derive the drought indices of water supply and demand, we used the ERA5L with a monthly frequency for 2000–2023. Drought indices capture historical anomalies of water supply and demand. To quantify each anomaly, the common practice is to derive it following a statistical parametric method in which it is assumed that the statistical distribution of the data is known⁶⁴. The use of an erroneous statistical distribution that does not fit the data is usually the highest source of uncertainty⁶⁵. In the case of Chile, due to its high degree of climatic variability, it is difficult to choose a statistical distribution that can be used across its entire extent. We therefore use a non-parametric method for the calculation of the drought indices, following ref. 66.

For monitoring water supply, we used the Standardized Precipitation Index (SPI; ref. 16), which only uses precipitation data. To evaluate water demand, we chose the Evaporative Demand Drought Index (EDDI; refs. 67, 24), which is based on AED, and the Standardized Evapotranspiration Index (SETI; ref. 25), which quantifies actual evapotranspiration, i.e. the amount of water removed from a surface due to evaporation and transpiration. To quantify the combined effect of water supply and demand, we estimated SPEI⁶⁸. For SPEI, we calculated an auxiliary variable (D) with the following formula:

$$D = P - AED \quad (2),$$

where P is precipitation. Soil moisture is often considered to be the main driver of vegetation productivity, particularly in semi-arid regions⁶⁹. Hence, we used the Standardized Soil Moisture Index (SSI) to analyze the change in soil moisture (SM)⁷⁰. For SSI, we used the average soil moisture from ERA5L at a depth of 1m. All calculated indices are multi-scalar and can be used for the analysis of short- to long-term droughts.

To derive the drought indices, we first calculated the sum of the variables for each time scale(s). In this case, for generalization purposes, we use V , referring to variables P , AED , D , ET , and SM (Table S2). We summed each variable over the time series (months), for a time scales s :

$$A_i^s = \sum_{i=n-s-i+2}^{n-i+1} V_i \quad \forall i \geq n - s + 1 \quad (3)$$

A_i^s corresponds to a moving window (convolution) that sums the variable for s . This is summed over s months, starting from the most recent month (n) back in time until month $n-s+1$. For example, using precipitation, a period of twelve months (n), and a time scale of three months (s):

$$A_1^3 = P_{oct} + P_{nov} + P_{dic}$$

$$\begin{aligned} & \vdots = \vdots + \vdots + \vdots \\ A_{10}^3 &= P_{jan} + P_{feb} + P_{mar} \end{aligned}$$

Then, we used the empirical Tukey plotting position⁷¹ over A_i^s to derive the $P(a_i)$ probabilities across a period of interest:

$$P(A_i^s) = \frac{i-0.33}{n+0.33} \quad (4)$$

We use an inverse normal approximation⁷² to obtain the empirically derived probabilities once the variable accumulates over time for the scale s . Thus, the drought indices *SPI*, *SPEI*, *EDDI*, and *SSI* are obtained in the following manner:

$$DI(A_i^s) = W - \frac{C_0 + C_1 \cdot W + C_2 \cdot W^2}{1 + d_1 \cdot W + d_2 \cdot W^2 + d_3 \cdot W^3}, \quad (5)$$

where *DI* refers to the drought index calculated for the variable V . The values for the constants are: $C_0 = 2.515517$, $C_1 = 0.802853$, $C_2 = 0.010328$, $d_1 = 1.432788$,

$d_2 = 0.189269$, and $d_3 = 0.001308$. For $P(A_i^s) \leq 0.5$, $W = \sqrt{-2 \cdot \ln(P(A_i^s))}$, and for $P(A_i^s) > 0.5$, replace $P(A_i^s)$ with $1 - P(A_i^s)$ and reverse the sign of $DI(A_i^s)$.

The drought indices were calculated for time scales of 1, 3, 6, 12, 24, and 36 months at a monthly frequency for 2000–2023.

Temporal trends of drought indices

To determine if there are statistically significant positive or negative temporal trends for the drought indices, we used the non-parametric modified Mann-Kendall test for serially correlated data⁷³. To determine the magnitude of the trend, we used Sen's slope⁷⁴. Sen's slope is less affected by outliers than parametric ordinary least squares (OLS) regression, and as a non-parametric method, it is not influenced by the distribution of the data. We applied both methods for *SPI*, *EDDI*, *SPEI*, *SETI*, and *SSI* and six time scales, resulting in a total of 30 trends. We then aggregated temporal trends for each ecoregion and land cover type.

Vegetation productivity

We also used the MODIS product (MOD13A3⁵²), to calculate vegetation productivity, and calculated anomalies of cumulative NDVI using $zcNDVI$ ⁴⁷, which was derived from the monthly time series of NDVI, with Equations 3, 4 and 5. For vegetation productivity, we selected the time scale that best correlates with annual net primary productivity (NPP) across continental Chile. For this purpose, we calculated $zcNDVI$ for time scales of 1, 3, 6, and 12 months (from December) and compared it with the annual NPP. We obtained NPP from MOD17A3HGF⁹⁰. We chose to use six months because the R^2 between $zcNDVI$ and NPP

reaches its highest value at six months, obtaining an R^2 of 0.31 for forest and 0.72 for shrubland (Supplementary Information Section S2). We subsequently used zcNDVI with a time scale of 6 months and calculated it at a monthly frequency for 2000–2023.

Drought impacts on vegetation productivity

For each land cover, we analyzed the trend of vegetation productivity. To this end, we identified areas within each land cover that are persistent over time to reduce the possibility that trends in vegetation productivity may be influenced by changes in land cover. We examined the correlation between drought indices and vegetation productivity across land cover types to determine to the extent to which soil moisture and water demand and supply affect vegetation productivity.

We estimated pixel-to-pixel Pearson's correlations between drought indices at time scales of 1, 3, 6, 12, 24, and 36 months with zcNDVI. We extracted the Pearson correlation coefficient corresponding to the time scale with the highest value. For each index, we then generated two maps: 1) a raster with values of the time scales and drought index that reached the maximum correlation (see Fig. S5), and 2) a raster with the magnitude of the correlation between the drought index and vegetation productivity.

Drought impacts on land cover change

Land cover change

To analyze land cover change, we used the classification scheme of the International Geosphere-Biosphere Programme (IGBP) from the product MCD12Q1 Collection 6.1 from MODIS. The MCD12Q1 product is produced for each year from 2001 to 2023 and defines 17 classes (see Table S1). Following the FAO classification⁷⁵, we classified native and planted forests as “forests”, which represent natural and productive ecosystems dominated by large trees. To analyze the land cover change, we use the IGBP scheme from the MCD12Q1 product. We regrouped the 17 classes into ten macro-classes, as follows: 1-4 to forests (native forest and plantations), 5-7 to shrublands, 8-9 to savannas, 10 as grasslands, 11 as wetlands, 12 and 14 to croplands, 13 as urban, 15 as snow and ice, 16 as barren, and 17 as water (Table S1). This resulted in a time series of land cover with ten macro-classes for 2001-2023. We validated the land cover macro-classes using a high resolution (30 m) land cover map for 2013-2014⁷⁶. Our results showed a global accuracy of ~0.82 and a F1 score of ~0.66 (Supplementary Information, S2).

We do not directly measure the change in land cover, but we analyze it indirectly. A decrease in one type of land cover leads to its replacement by another, and an increase in a particular land cover class means it is replacing other types of covers. Thus, we calculated the area for each land cover class in the five ecoregions for 2001–2023. We then estimated the temporal change in area for each land cover type macroclass and determined the statistical significance (p -value < 0.05) and magnitude of the trend, as described above.

To assess how water demand and supply, and soil moisture affect the variation in vegetation productivity across various land cover types, we avoid analyzing areas that experienced major land cover changes in the 2001–2023 period. To assess how zcNDVI varied

irrespective of land cover change, we developed a persistence mask for land cover, which only retains pixels for which the macro-class remained the same for at least 80% of the 23 years (Fig. 1d).

Relationship between land cover and drought trends

To identify which drought indices and time scales have a major impact on changes in land cover type, we examined the relationships between the temporal trends in the surface of land cover classes, drought indices, road density, burned area, and night lights, and for each ecoregion. We performed the analysis at the sub-basin scale, using 485 river basins, which have a surface area between 0.906 and 24,408 km² and a median area of 1,249 km² (Supplementary Fig. S3/Table S3). For each basin, we calculated the trend per land cover, considering the proportion of the type relative to the total surface of the basin. For each basin we extracted the average trend of all drought indices and at time scales of 1, 3, 6, 12, 24, and 36 months. In the case of burned area, we used as variables the total and the trend of burned area for 2002-2023, and for nightlights we used the average and the trend of nightlights for 2012-2023.

Prior to modelling relationships between trends in land cover and drought indices, we assessed multi-collinearity among explanatory variables, i.e., drought indices, road density, night lights, and burned area, with the variance inflation factor (VIF). We analyzed the VIF for all drought indices at time scales of 1, 3, 6, 12, 24, and 36 separately because each index has a strong correlation across time scales. As VIF values greater than five may affect the interpretation of model results⁷⁷, we therefore excluded SPI from all subsequent models.

To assess the relationship between land cover trends and drought indices, we modeled trends in the surface of land cover types. We made a regression analysis using the random forest method⁹³, which employs multiple decision trees. Some advantages of random forest include the ability to find non-linear relationships, reduce overfitting, and derive variable importance. We incorporated the trends of the five drought indices (SPI, SPEI, EDDI, SETI, and SSI), the nightlights (trend and average) and burned area (trend and total area), the road density, for a total of ten predictors. We then constructed random forest models for each time scale (1, 3, 6, 12, 24, and 36) and each land cover class (forest, grassland, shrubland, savanna, cropland, and barren land), resulting in a total of 36 RF models. We trained each model using 1000 trees, setting the minimum number of nodes per decision tree at five and the number of predictors per split (boosting) to the square root of the total number of predictors. To account for uncertainty, we trained all the models ten times using a resampling strategy (ten folds) in a cross-validation scheme. Finally, we evaluate model fit by calculating R², root mean square error (RMSE), and variable importance. Variable importance identifies which variables have a higher contribution to explaining model variation. We calculated variable importance by permuting out-of-bag (OOB) data per tree and calculating the mean standard error of the OOB data. After permuting each predictor variable, we repeated the process for the remaining variables. We repeated this process ten times per model (ten folds) to assess model fit while accounting for uncertainty in model performance.

Finally, we visually explored the relationship between drought indexes and changes in land cover across sub basins within Chile. To achieve this, we compared the relative changes in land cover surface with the drought indices, burned area, nightlights, and road density for the time scale that was deemed more significant in the random forest model that reached the highest r-squared per land cover type.

Software

For downloading, processing, and analyzing spatio-temporal data, we used the R programming language for statistical computing and graphics⁷⁸. For downloading ERA5L, we used the {ecmwf} package⁷⁹. For processing raster data, we used {terra}⁸⁰ and {stars}⁸¹. For managing vectorial data, we used {sf}⁸². For the calculation of AED, we used {SPEI}⁸³. For mapping, we used {tmap}⁸⁴. For data analysis and visualization, the suite {tidyverse}⁸⁵ was used. For the random forest modeling, we used the {tidymodels}⁸⁶ and {ranger}⁸⁷ packages.

Results

The Chilean matorral and Patagonian steppe increase atmospheric water demand but decrease vegetation evapotranspiration

Overall, we found that generally, the majority of the drought indices indicate that the temporal trends (positive or negative) intensify over longer time periods (Fig. 2). For the Atacama Desert and the Central Andean dry puna, we found a positive temporal trend for drought indices of water supply (i.e., SPI and SSI), atmospheric water demand (i.e., EDDI), and vegetation water demand (i.e., SETI). For the Chilean Matorral and Patagonian steppe, EDDI becomes increasingly positive, while SPI, SPEI, SSI, and SETI become increasingly negative. This reflects a critical scenario of drought, where a rise in temperature increases atmospheric water demand, but vegetation cannot increase evapotranspiration due to a lack of water availability. In the Southern Andean steppe, there is a positive temporal trend in AED (i.e., EDDI), but a negative temporal trend in water supply (i.e., SPI, SPEI, SSI). The negative temporal trend in vegetation water demand (i.e., SETI) strengthens with longer time scales. The Valdivian temperate forests show a negative temporal trend in water supply (i.e., SPI, SPEI, and SSI) and a positive trend in both AED and ET, as shown by EDDI and SETI, respectively. In this case, an increase in AED implies an increase in ET, likely due to a greater availability of water, unlike in the Chilean Matorral and Patagonian steppe. The vegetation water demand (SETI) in the Magellanic subpolar forests does not exhibit a significant trend over any given time scale, while AED and water supply become increasingly positive over longer time scales. The trends of drought indices in the Patagonian steppe exhibit a similar behavior to the Chilean Matorral, albeit less extreme.

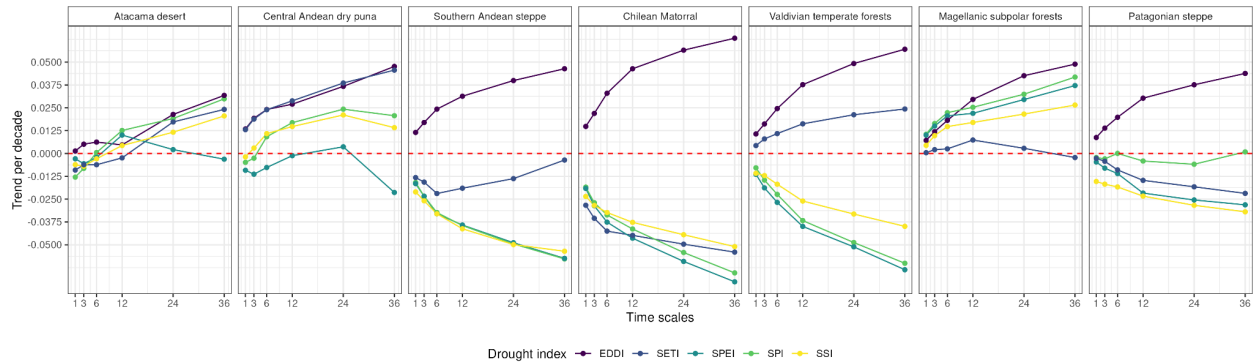


Figure 2. The Chilean Matorral and Patagonian steppe show a higher increase in atmospheric water demand and a decrease in vegetation evapotranspiration, which becomes stronger at longer time scales. Temporal trends in drought intensity over multiple time scales for indices associated with water supply (SPI, SPEI, SSI), atmospheric water demand (EDDI) and vegetation water demand (SETI) across continental Chile for 2000-2023. SPI is the standardized precipitation index, SPEI is the Standardized Precipitation Evapotranspiration Index, SSI is the Standardized Soil Moisture Index, EDDI is the Evaporative Demand Drought Index, and SETI is the Standardized Evapotranspiration Index. Drought indices were aggregated per region for visualization. All temporal trends are statistically significant ($p < 0.05$).

Vegetation productivity has strongly decreased in the Chilean matorral and the Patagonian steppe

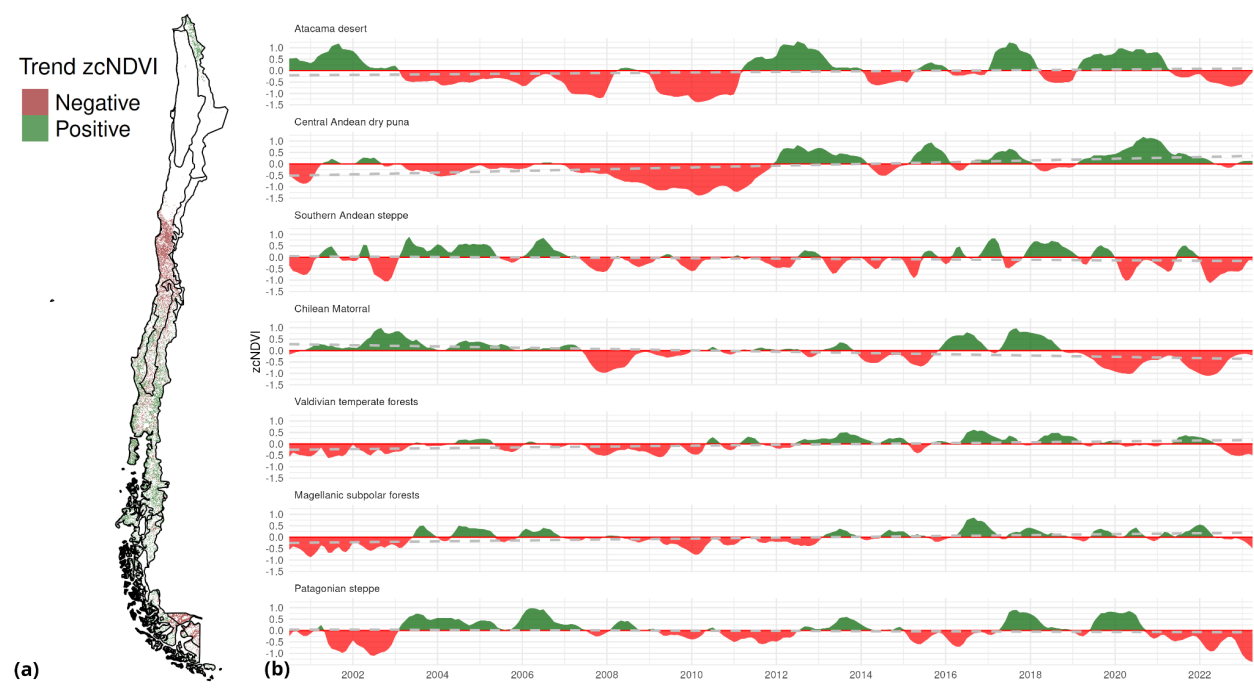


Figure 3. The Chilean matorral and Patagonian steppe have experienced the greatest decline in vegetation productivity. Spatial (a) and temporal (b) variation in vegetation productivity across continental Chile for 2000-2023. Vegetation productivity was estimated as standardized vegetation productivity (zcNDVI). In (a) green corresponds to areas with a positive trend in zcNDVI, and red corresponds to a negative temporal trend in zcNDVI. In (b), red areas correspond to negative and green to positive intensity of zcNDVI. Temporal trends in zcNDVI were estimated with the non-parametric modified Mann-Kendall test for serially correlated

data. The white space on the map represents areas without persistent land cover, or areas where there is no significant trend. All temporal trends shown are statistically significant ($p < 0.01$).

We found contrasting temporal trends in vegetation productivity for 2000-2023 across ecoregions (Fig. 3). While the Atacama desert does not exhibit significant temporal trends in vegetation productivity, that of the Chilean Matorral, Patagonian steppe, and the Southern Andean steppe exhibit negative trends of -0.023, -0.016, and -0.006 (z-score per decade), respectively. In contrast, the Central Andean dry puna, Valdivian temperate forests, and Central Andean dry puna show positive temporal trends in zcNDVI ranging from 0.01 to 0.03 (z-score per decade). The Chilean Matorral reached its lowest point from 2019 to 2022, while the Patagonian steppe has experienced an increasingly negative trend in vegetation productivity since 2022.

Forest, savanna, and shrubland exhibit the highest change in surface area across ecoregions

We also observed significant changes in land cover across continental Chile (Fig. 4). The forest surface area increased in the Chilean matorral and in the Valdivian temperate forest at rates of 78 and 316 $\text{km}^2 \text{yr}^{-1}$, respectively. Grassland surface area has diminished in the Southern Andean steppe (-19 $\text{km}^2 \text{yr}^{-1}$), yet has increased in the Patagonian steppe (90 $\text{km}^2 \text{yr}^{-1}$). Savanna has decreased rapidly in the Chilean matorral at a rate of -271 $\text{km}^2 \text{yr}^{-1}$ and in the Valdivian temperate forest at a rate of -276 $\text{km}^2 \text{yr}^{-1}$, but has increased at a rate of 133 $\text{km}^2 \text{yr}^{-1}$ in the Magellanic subpolar forest. Among land cover types, shrubland surface area has increased the most in the Chilean matorral (160 $\text{km}^2 \text{yr}^{-1}$). Barren land has increased at moderate rates in the Central Andean dry puna (36 $\text{km}^2 \text{yr}^{-1}$) and the Southern Andean steppe (50 $\text{km}^2 \text{yr}^{-1}$), but has diminished in the Magellanic subpolar forest (-81 $\text{km}^2 \text{yr}^{-1}$).

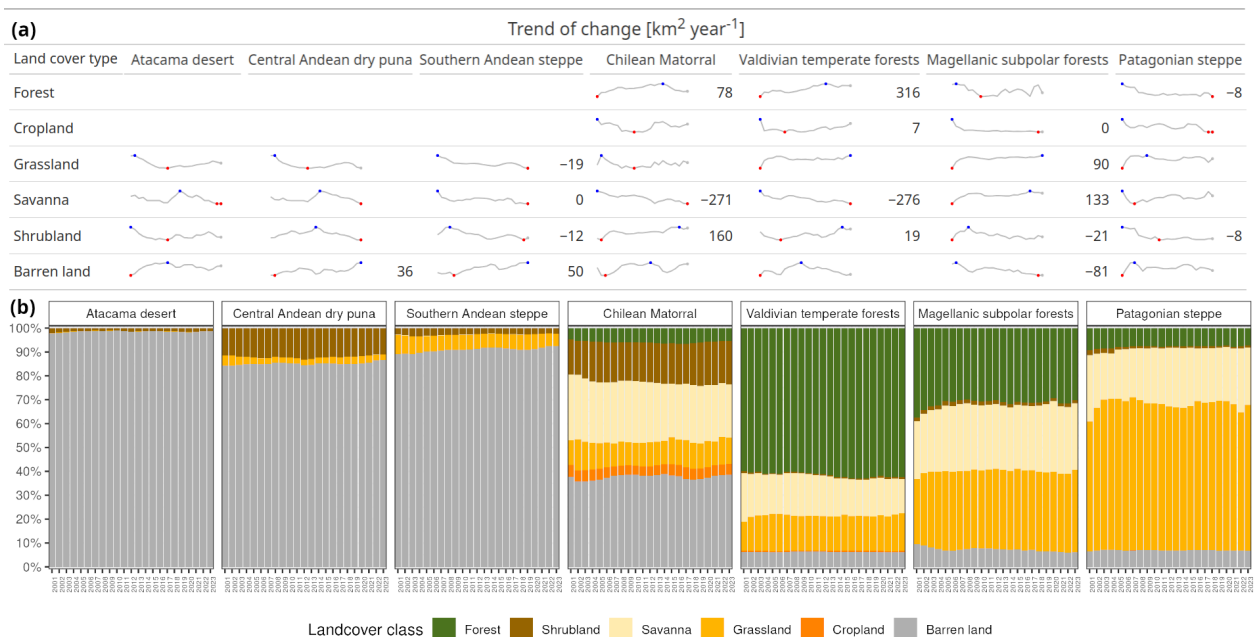


Figure 4. Land cover is shifting dynamically across continental Chile. Temporal trends in absolute (a) and relative (b) land cover change in surface across continental Chile for 2001-2023. Temporal change in area for

each class was estimated with Sen's slope; zero values indicate no change, curves without values show no significant trend, while red and blue points indicate maximum and minimum values, respectively. Land cover classes with no values indicate that in that ecoregion there was not a significant surface with the land cover type. Relative land cover change was estimated within each ecoregion.

Drought impacts on vegetation productivity are strongest in the Chilean Matorral and Valdivian temperate forest

Our results indicate that drought impacts on vegetation productivity are highest in the Chilean Matorral and Valdivian temperate forests across all land cover types, except forest (Figs. 5 & S5 and Table 1). For time scales of 6 and 12 months, SETI and SSI have the strongest positive correlation with vegetation productivity among the land cover types. Next, we found that grassland and savanna in the Patagonian steppe had higher correlations with SPI and SSI over a time scale of 12 months. Further, there is a positive relationship between vegetation productivity in the Atacama desert and drought indices of 12 months of water supply and vegetation water demand. However, there is a negative relationship between vegetation productivity and atmospheric water demand over a time scale of 12 months. All drought indices show a positive correlation with vegetation productivity in the Central Andean dry puna, particularly for the drought indices of water supply (SPI, SPEI, and SSI) at a time scale of 24 months and vegetation water demand (SETI) at a time scale of 36 months. For the Southern Andean steppe the SETI at a time scale of 24 months showed the highest correlation with vegetation productivity in savannas, followed by the EDDI at a time scale of 24 months.

Our analysis also revealed that water demand and supply differentially affected the time scales at which vegetation productivity of land cover types within each region was most impacted by drought (Figs. 5 & S5 and Table 1). While the spatial variation in the relationship between drought intensity and vegetation productivity was consistent across drought indices, the drought indices that captures water supply *via* soil moisture (Standardized Soil Moisture Index; SSI), and *via* vegetation water demand (Standardized Evapotranspiration Index, SETI) tended to show a stronger correlation with vegetation productivity over larger areas than the other drought indices (Fig. 5).

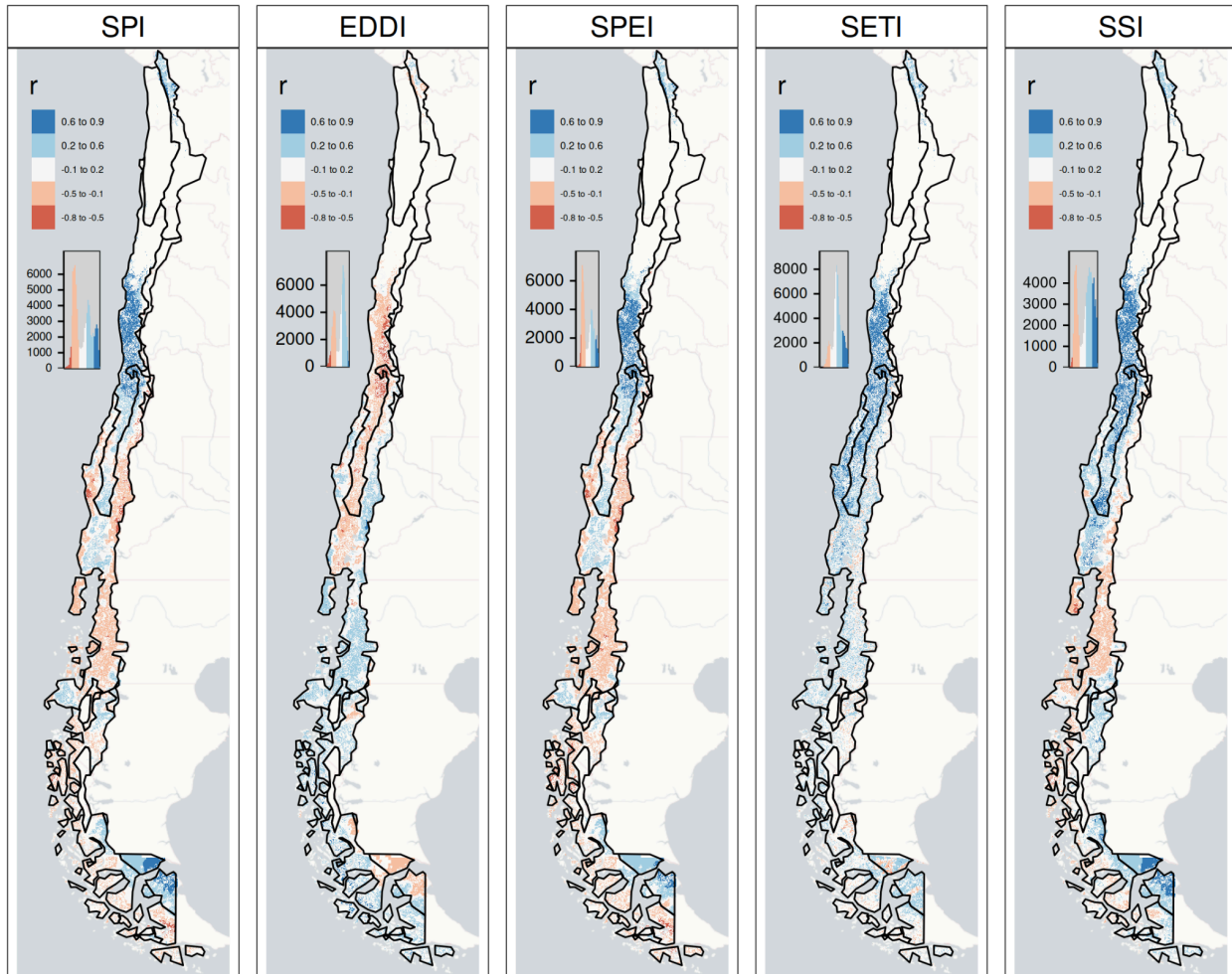
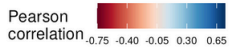


Figure 5. Drought impacts on vegetation productivity shift across continental Chile. Pearson's correlation coefficient was used to estimate the direction and magnitude of the relationship between drought severity and vegetation productivity for each index for 2000-2023. We show Pearson correlation coefficients for the time scale (3 - 36 months) at which they reach their maximum absolute value. In Chile, areas in white indicate no statistically significant correlation (p -value >0.05). SPI is the standardized precipitation index, SPEI is the Standardized Precipitation Evapotranspiration Index, SSI is the Standardized Soil Moisture Index, EDDI is the Evaporative Demand Drought Index, and SETI is the Standardized Evapotranspiration Index.

Table 1. Time scale at which drought indices (EDDI, SPI, SPEI, SSI, and SETI) exhibit the maximum absolute correlation with vegetation productivity (zcNDVI) across continental Chile. The numbers in each cell indicate the time scale in months (1, 3, 6, 12, 24, and 36 months) at which the maximum absolute correlation between a drought index and vegetation productivity (zcNDVI) occurs, and the color indicates the strength of the correlation. Cells without values signify that either the correlation was not statistically significant, or that a given land cover type is not present in a particular ecoregion.

Ecoregion	Forest					Cropland					Grassland					Savanna					Shrubland				
	EDDI	SPEI	SPI	SSI	SETI	EDDI	SPEI	SPI	SSI	SETI	EDDI	SPEI	SPI	SSI	SETI	EDDI	SPEI	SPI	SSI	SETI	EDDI	SPEI	SPI	SSI	SETI
Atacama desert											12	12	12	12	12	6	12	12		12	12	12	12	12	12
Central Andean dry puna											12	36	36	36	36	24	36	36	36	36	12	36	36	36	12
Southern Andean steppe											24	12	12	6	6	24	12	12	6	24	6	36	36	36	6
Chilean Matorral	6	6	6	6	6	6	12	12	6	6	36	24	24	12	12	6	12	12	6	6	36	24	24	12	12
Valdivian temperate forests	6	6	6	12	36	6	6	6	6	6	6	12	12	12	6	6	6	24	6	6	36	12	12	12	12
Magellanic subpolar forests	6		36	6	6	12	12	12	36	24	6	12	12	6	6	6	6	6	6	6	6	6	6	36	6
Patagonian steppe	6	6	12	36	12						12	12	12	12	12	36	12	12	12	24		12	12	36	



Drought strongly impacts land cover distribution for shrublands

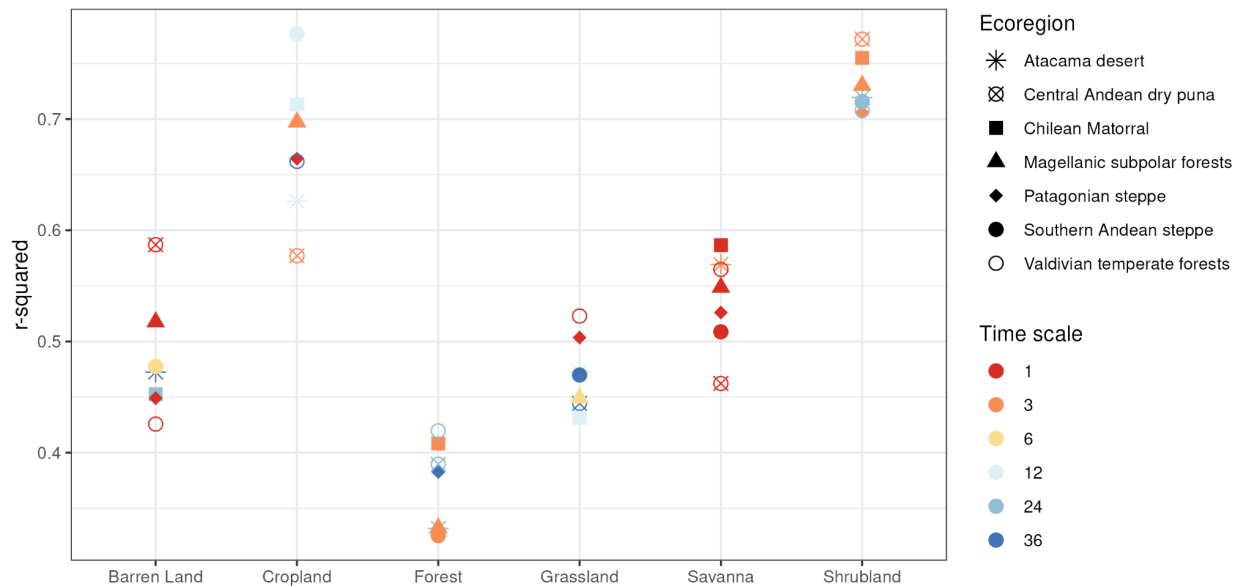


Figure 6. Shifts in shrubland areas are sensitive to drought time scales of three and 12 months. The random forest per land cover class over the ecoregions achieves an R-squared value per time scale of the drought index. The time scales correspond to the time scale of the index that reached the higher r-squared.

Our random forest models explain between 32-79% of variation in the temporal trend of land cover change across continental Chile (Fig. 6). These results highlight the importance of considering water supply (e.g., SPEI and SSI) and demand (e.g., SETI), as drought indices associated with both aspects of the water balance had high importance values across most ecoregions and land cover types. The variation in the time scale of drought indices with

high importance values may suggest that different types of vegetation are not equally sensitive to droughts of similar intensities (Fig. 6).

Our RF models show that the drought indices explain between 71 and 78% of the variation in temporal trends of land cover surface change for shrublands across all ecoregions (Fig. 6). Further, our RF models explain approximately 58 to 78% of the variation in the temporal trend of land cover change for croplands. In the case of other land cover types, the RF models account for approximately 33-59% of the variation in temporal trends of land cover change, with drought indices explaining less variation in land cover change for forests than other land cover types (Fig. 6).

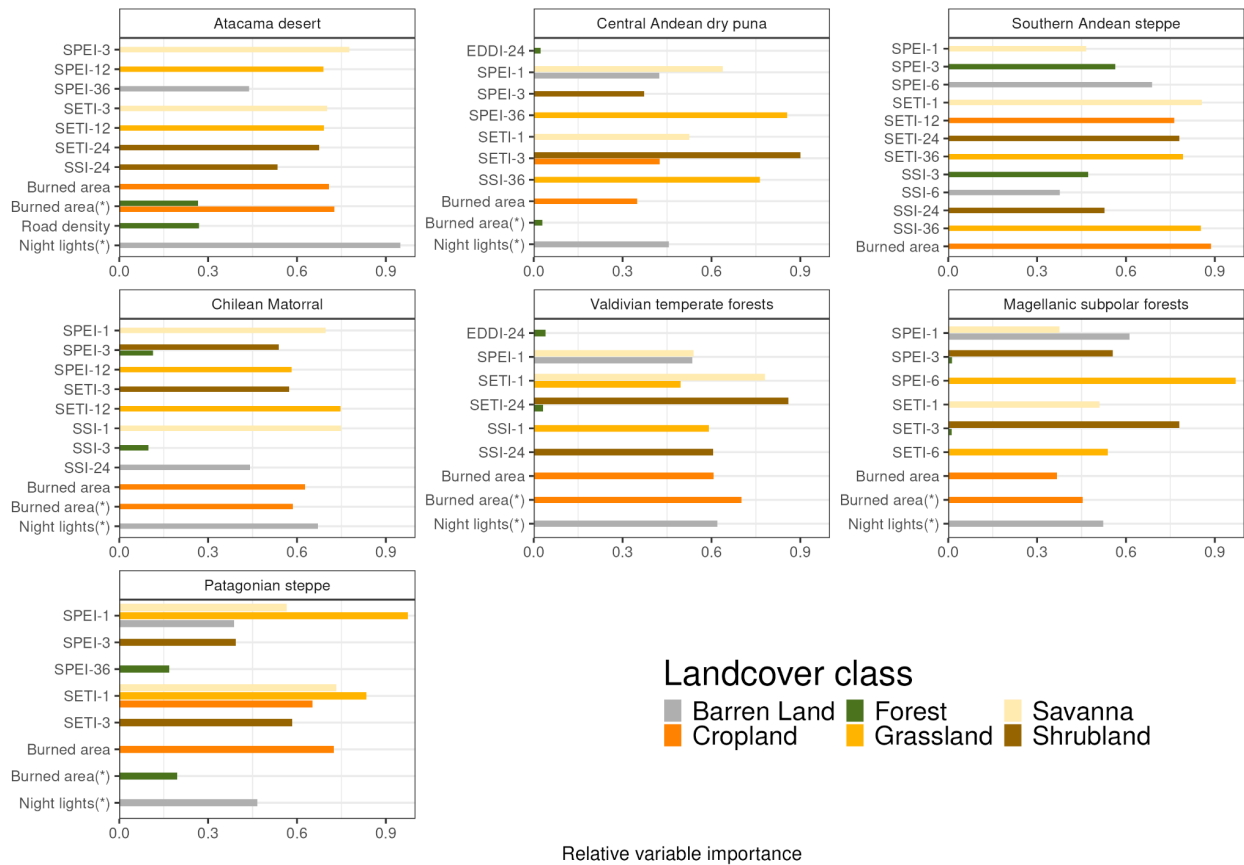


Figure 7. Shifts in water supply and demand are the main factors that drive land cover change. Variable importance of multi-scalar drought indices for explaining land cover change in ecoregions across continental Chile. Variable importance was estimated with Random Forest models fitted for each combination of land cover type. SPEI is the Standardized Precipitation Evapotranspiration Index, SETI is the Standardized Evapotranspiration Index, SSI is the Standardized Soil Moisture Index, Night Lights(*) is the average night lights for 2012-2023, Burned Area is the trend in surface burned for 2002-2023, and Burned Area(*) is the total surface affected by fires between 2002 and 2023. Note that we only show the two explanatory variables with the highest variable importance values for each land cover type.

We found the highest R-squared for the RF model explaining variation in the temporal trend of land cover change for shrublands, followed by that of croplands and barren land (Fig. 6). Our models most frequently identified SETI and SSI as the drought indices that explained the highest amount of variation in the temporal trend of land cover change (Fig. 7). Across

all ecoregions, we found that the total surface of burned area or the temporal trend of burned area explained relatively more variation in the temporal trend of land cover change for croplands than drought indices, as well as other variables associated with human activity (Fig. 7). Similarly, we found that nighttime lights emissions, a proxy for human population density and density of built structures, explained relatively more variation in the temporal trend in the land cover change of barren land, followed SPEI at time scales of 3 and 6 months (Fig. 7).

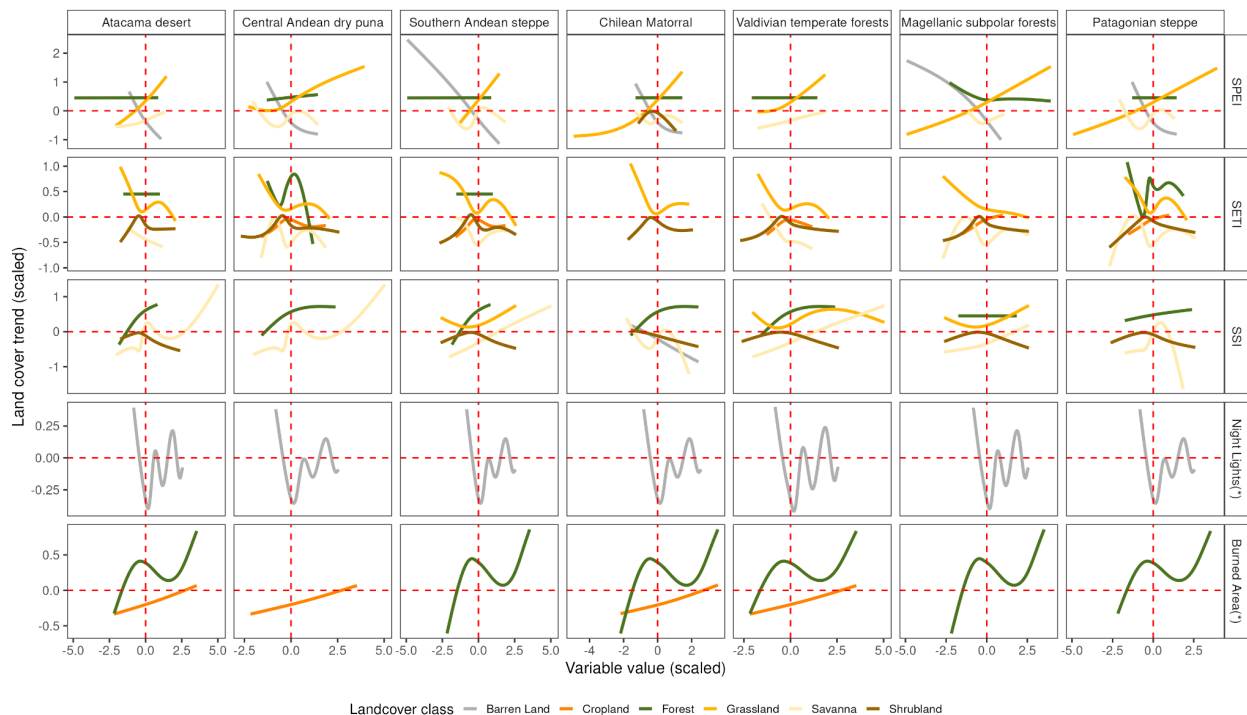


Figure 8. Drought intensity drives land cover change, but not for all cover types. Response of land cover change in response to water demand and supply across multiple time scales and ecoregions in continental Chile. SPEI is the Standardized Precipitation Evapotranspiration Index, SETI is the Standardized Evapotranspiration Index, SSI is the Standardized Soil Moisture Index, and Night Lights(*) is the average night lights for 2012-2023, and Burned Area(*) is the total surface affected by fires between 2002 and 2023. For SPI, SPEI, SETI, and SSI, negative values are associated with more severe drought. Fitted lines are smoothed response curves across river basins in each region estimated with Random Forest models.

In general, our results indicate that increases in SPEI, SETI, and SSI were associated with non-linear increases in the temporal trends of land cover change for most types of land cover (Fig. 8). We observed that shrublands are sensitive to both increases and decreases in SETI and SSI, reaching a point of equilibrium around a normal climatic situation (drought index = 0). Surprisingly, we found that the temporal trend in the land cover change of forests was stable for both SPEI and SETI for most ecoregions, only increasing non-linearly with increasing SSI. In the case of bare soil, we found a negative relationship between the temporal trend in land cover and nighttime light emissions, such that areas with an increase in barren land are associated with a low amount of nighttime light emissions. We found that SETI and SPEI had contrasting impacts on the temporal trend in the land cover change of

grasslands, which increased in response to increasing SPEI yet decreased in response to increasing SETI.

Discussion

Temporal trends in water supply and demand

We discovered that the Atacama desert, Central Andean dry puna, and the Magellanic subpolar forests experience an increase in water supply (SPI, SSI), as well as an increase in atmospheric and vegetation water demand (EDDI, SETI). However, in the Magellanic subpolar forests, we found no evidence of either a significant increase or decrease in SETI across time scales. Also, we found a significant decreasing trend in water supply (SPI, SPEI, and SSI) across the Southern Andean steppe, Chilean Matorral^{88,89}, Valdivian temperate forests, and Patagonian steppe, accompanied by an increase in atmospheric water demand (EDDI). Our results indicate that temporal trends of water supply and atmospheric demand tend to decrease or increase more strongly over longer time scales, a trend that is consistent with the progressive intensification of drought severity across much of Chile, and that has been observed in other regions facing long-term droughts^{90,91}. Simultaneously, we observed a divergent trend between EDDI and SETI. In the majority of ecoregions, a rise in atmospheric water demand (EDDI) typically leads to a rise in vegetation water demand (SETI). However, in the ecoregions most affected by drought (Fig. 3 and Fig. 5), i.e., the Chilean matorral, and the Patagonian steppe, we found that an increase in atmospheric water demand results in a decrease in the water demand of vegetation. Together, our findings demonstrate a persistent drying trend in the Chilean Matorral, the Patagonian steppe, and the Southern Andean steppe. We attribute this trend to a simultaneous decrease in precipitation and an increase in atmospheric evaporative demand, leading to a decrease in the water demand by vegetation in water-limited areas⁹².

Temporal trends in vegetation productivity

The consequences of the persistent drying trend for ecosystems throughout continental Chile are manifold. First, the prolonged hydrological drought, i.e., precipitation deficit, has reduced groundwater storage (SSI; ref. 93), leading to a steady decline in vegetation productivity (zcNDVI) since 2000 across the Patagonian steppe, the Southern Andean steppe, and the Chilean Matorral, which reached its lowest level between 2020 and 2022 and could be due to either a decrease in vegetation area, a loss of biomass, or browning in forest ecosystems. Recent studies examining natural and productive ecosystems⁹⁴⁻⁹⁶ have attributed the decline in vegetation productivity with declines in soil moisture and increases in evapotranspiration. Second, the sharp decline in vegetation productivity in the Chilean Matorral and Valdivian temperate forest ecoregions showed that grasslands and shrublands respond to shifts in water supply over longer time scales (12 months) than savannas and croplands (6 months). Also, in the Valdivian temperate forest ecoregion, which has a large forested area, vegetation productivity responded to soil moisture (SSI) and vegetation water demand (SETI) most strongly at 12 and 36 months, respectively. This result is consistent with recent studies showing that progressive, long-term water deficits in central Chile have triggered forest browning and declines in native forest productivity^{1,43,97}. While our analysis do not distinguish between native and planted forests, the latter of

which are considered to be more drought tolerant in central and southern Chile⁹⁸, we show that forest area declines more sharply in response to increasing water demand due to rising temperatures (EDDI) than decreasing water supply (e.g., SPI, SSI; refs. 99, 100), which may have cascading impacts on multiple facets of forest diversity^{101, 102}.

Moreover, the strengthening of the correlation between vegetation productivity and water supply (SPI, SPEI, SSI) or demand (EDDI, SETI) over multiple time scales (up to 36 months) and across land cover types (Fig. 5) demonstrates the impacts of climate change on the water balance in Chile. These impacts may extend beyond vegetation productivity, as reduced soil moisture in central Chile and the western United States has increased wildfire activity^{103, 104}, which is a growing concern in Chile and may be further exacerbated by extensive plantations of highly flammable tree species, e.g., *Eucalyptus* spp. and *Pinus* spp.¹⁰⁵. Lastly, we found that the decline in the vegetation productivity of croplands is largely due to a decrease in the water supply and vegetation water demand to a greater extent than to an increase in atmospheric water demand¹⁰⁶, causing a decline in water availability. This is consistent with evidence that more water-intensive crops have replaced less water-intensive crops in central Chile, leading to an increase in water extraction from rivers or groundwater^{107, 108}.

Drought impacts on land cover

We found evidence that temporal decreases in water supply (SPEI, SSI) and decreases in vegetation water demand (SETI) are driving shifts not only in vegetation productivity but also in temporal trends of land cover change across most of continental Chile. Despite differences in drought tolerance (e.g., shrublands, grasslands, and savannas), our results provide evidence that the area of most land cover types dominated by vegetation has been affected by water deficits, albeit to varying degrees (Fig. 8). Additionally, our results suggest that water deficits, to a greater extent than factors associated with human activity, have affected temporal trends in land cover change for most land cover types. Further, we found that temporal changes in cropland cover may not be a direct consequence of drought (Fig. 7), but rather an indirect one, likely associated with forest fires and possibly the decisions of resource-poor farmers to migrate to regions with more abundant water resources or to change economic activity^{10, 109}. The reason for the non-linear increases in forest area in response to burned area across most ecoregions (Fig. 8) is unclear, as it could be due to forest recovery⁴⁴ or the establishment of forest plantations¹¹⁰.

Study limitations

Our analysis of the impacts of water supply and demand on vegetation productivity and land cover change has some important limitations that need to be highlighted. One of the principal limitations of this study is the use of secondary information. For instance, we used estimates of water supply and demand, such as ERA5L and MODIS, which, despite their improved estimation capacity, suffer from biases and uncertainties^{111, 112} in different areas or climatic conditions. In this study, we compared the ERA5L data with climatic stations (see Table S2) to verify bias and uncertainty, but future studies that aim for more focalized analysis will need to improve the precision of these products. We used zcNDVI⁴⁷ (MODIS) as

a proxy for vegetation productivity, which has proven to be a good estimate of NPP (see Fig. S1 and S2), but its quality varies between different types of vegetation.

A second limitation is that we used products that estimate land cover types using classification models, which are subject to quality errors that must be taken into account^{113, 114}. In addition, in our case we used macro classes of land cover, where, for example, the different types of forests (e.g., monoculture, native forest) were pooled into the same land cover type. This approach may hinder our ability to understand the effects of drought on the various subclasses within each land cover class. In terms of croplands, we could not distinguish between rainfed and irrigated areas using macro classes. However, in this study, we aimed to provide a broad overview at a large spatial scale, but acknowledge that using sub-classes of land cover types at finer spatial resolutions may help to better understand underlying mechanisms.

In our analysis of the impacts of drought intensity on temporal trends of land cover change, we integrated proxies for human activity that also may affect land cover change. However, attributing land cover change to human activity and decisions is complex when using earth observation tools. While earth observation tools can analyze land cover change, whether a land cover type changes likely depends on a multitude of social and economic factors that are challenging to quantify^{115, 116} and necessitate the integration of social, natural, and geographic information sciences.

Conclusion

Overall, our results show that long-term declines in water supply and demand have consistently induced widespread, multi-dimensional impacts on the vegetation productivity and on the temporal trends of changes in land cover types across a broad range of ecoregions. While prolonged droughts may directly cause shifts to more drought-tolerant land cover types, such as shrublands, we also found that areas affected by fires were associated with increases in the area of forests and croplands, highlighting the importance of socio-economic factors in shaping land use change dynamics. Our study extends current understanding of drought impacts by demonstrating how their multidimensionality emerges over multiple time scales and across land cover types, which can contribute to developing context-specific adaptation strategies for agriculture, biodiversity conservation, and natural resource management.

Data availability

The codes generated during the current study are available in the GitHub repository, https://github.com/FSEQ210022/drought_vegetation. The datasets generated and/or analyzed during the current study are available in the Zenodo repository, <https://doi.org/10.5281/zenodo.10359547>.

Acknowledgments

The National Research and Development Agency of Chile (ANID) funded this study through the drought emergency project FSEQ210022, Fondecyt Iniciación N°11190360, Fondecyt Postdoctorado N°3230678, and Fondecyt Regular N°1210526.

References

1. Miranda, A. et al. Widespread synchronous decline of Mediterranean-type forest driven by accelerated aridity. *Nature Plants* 9, 1810–1817 (2023). URL <https://www.nature.com/articles/s41477-023-01541-7>.
2. Calvin, K. et al. IPCC, 2023: Climate Change 2023: Synthesis Report. Contribution of Working Groups I, II and III to the Sixth Assessment Report of the Intergovernmental Panel on Climate Change [Core Writing Team, H. Lee and J. Romero (eds.)]. IPCC, Geneva, Switzerland. Tech. Rep., Intergovernmental Panel on Climate Change (IPCC) (2023). URL <https://www.ipcc.ch/report/ar6/syr/>.
3. Cheng, Y. et al. Scattered tree death contributes to substantial forest loss in California. *Nature Communications* 15, 641 (2024). URL <https://www.nature.com/articles/s41467-024-44991-z>.
4. Crausbay, S. D. et al. Defining Ecological Drought for the Twenty-First Century. *Bulletin of the American Meteorological Society* 98, 2543–2550 (2017). URL <https://journals.ametsoc.org/view/journals/bams/98/12/bams-d-16-0292.1.xml>. Publisher: American Meteorological Society.
5. Mishra, A. K. & Singh, V. P. A review of drought concepts. *Journal of Hydrology* 391, 202–216 (2010). URL <https://linkinghub.elsevier.com/retrieve/pii/S0022169410004257>.
6. Van Loon, A. F. Hydrological drought explained. *WIREs Water* 2, 359–392 (2015). URL <https://wires.onlinelibrary.wiley.com/doi/10.1002/wat2.1085>.
7. Van Loon, A. F. et al. Drought in a human-modified world: reframing drought definitions, understanding, and analysis approaches. *Hydrology and Earth System Sciences* 20, 3631–3650 (2016). URL <https://hess.copernicus.org/articles/20/3631/2016/>.
8. Wilhite, D. A. & Glantz, M. H. Understanding: The drought phenomenon: The role of definitions. *Water International* 10, 111–120 (1985). URL <http://dx.doi.org/10.1080/02508068508686328>.
9. Van Loon, A. F. et al. Drought in the Anthropocene. *Nature Geoscience* 9, 89–91 (2016).
10. AghaKouchak, A. et al. Anthropogenic Drought: Definition, Challenges, and Opportunities. *Reviews of Geophysics* 59, e2019RG000683 (2021). URL <https://agupubs.onlinelibrary.wiley.com/doi/10.1029/2019RG000683>.
11. Lawler, J. J. et al. Projected land-use change impacts on ecosystem services in the United States. *Proceedings of the National Academy of Sciences* 111, 7492–7497 (2014). URL <https://pnas.org/doi/full/10.1073/pnas.1405557111>.
12. Newbold, T. et al. Global effects of land use on local terrestrial biodiversity. *Nature* 520, 45–50 (2015). URL <https://www.nature.com/articles/nature14324>.
13. Vicente-Serrano, S. M. et al. Global drought trends and future projections. *Philosophical Transactions of the Royal Society A: Mathematical, Physical and Engineering Sciences* 380, 20210285 (2022). URL <https://royalsocietypublishing.org/doi/10.1098/rsta.2021.0285>.
14. Kogan, F., Guo, W. & Yang, W. Near 40-year drought trend during 1981–2019 earth warming and food security. *Geomatics, Natural Hazards and Risk* 11, 469–490 (2020). URL <https://www.tandfonline.com/doi/full/10.1080/19475705.2020.1730452>.
15. WMO, Svoboda, M., Hayes, M. & Wood, D. A. Standardized Precipitation Index User Guide (WMO, Geneva, 2012).
16. Mckee, T. B., Doesken, N. J. & Kleist, J. The relationship of drought frequency and duration to time scales. In: *Proceedings of the Ninth Conference on Applied Climatology*. American Meteorological Society 179–184 (1993).
17. Vicente-Serrano, S. M., McVicar, T. R., Miralles, D. G., Yang, Y. & Tomas-Burguera, M. Unraveling the influence of atmospheric evaporative demand on drought and its response to climate change. *WIREs Climate Change* 11, e632 (2020). URL <https://wires.onlinelibrary.wiley.com/doi/10.1002/wcc.632>.
18. Gebrechorkos, S. H. et al. Global high-resolution drought indices for 1981–2022. *Earth System Science Data* 15, 5449–5466 (2023). URL <https://essd.copernicus.org/articles/15/5449/2023/>.
19. Liu, X., Yu, S., Yang, Z., Dong, J. & Peng, J. The first global multi-timescale daily SPEI dataset from 1982 to 2021. *Scientific Data* 11, 223 (2024). URL <https://www.nature.com/articles/s41597-024-03047-z>.
20. Narasimhan, B. & Srinivasan, R. Development and evaluation of Soil Moisture Deficit Index (SMDI) and Evapotranspiration Deficit Index (ETDI) for agricultural drought monitoring. *Agricultural and Forest Meteorology* 133, 69–88 (2005). URL <https://linkinghub.elsevier.com/retrieve/pii/S0168192305001565>.
21. Souza, A. G. S. S., Ribeiro Neto, A. & Souza, L. L. D. Soil moisture-based index for agricultural drought assessment: SMADI application in Pernambuco State-Brazil. *Remote Sensing of Environment* 252, 112124 (2021). URL <https://linkinghub.elsevier.com/retrieve/pii/S0034425720304971>.

22. AghaKouchak, A. A baseline probabilistic drought forecasting framework using standardized soil moisture index: application to the 2012 United States drought. *Hydrology and Earth System Sciences* 18, 2485–2492 (2014). URL <https://hess.copernicus.org/articles/18/2485/2014/>.
23. AghaKouchak, A. et al. Remote sensing of drought: Progress, challenges and opportunities. *Reviews of Geophysics* 53, 452–480 (2015). URL <http://dx.doi.org/10.1002/2014RG000456>.
24. McEvoy, D. J. et al. The Evaporative Demand Drought Index. Part II: CONUS-Wide Assessment against Common Drought Indicators. *Journal of Hydrometeorology* 17, 1763–1779 (2016). URL <http://journals.ametsoc.org/doi/10.1175/JHM-D-15-0122.1>.
25. Yang, T., Ding, J., Liu, D., Wang, X. & Wang, T. Combined Use of Multiple Drought Indices for Global Assessment of Dry Gets Drier and Wet Gets Wetter Paradigm. *Journal of Climate* 32, 737–748 (2019). URL <https://journals.ametsoc.org/doi/10.1175/JCLI-D-18-0261.1>.
26. Camps-Valls, G. et al. A unified vegetation index for quantifying the terrestrial biosphere. *Science Advances* 7, eabc7447 (2021). URL <https://www.science.org/doi/10.1126/sciadv.abc7447>.
27. Paruelo, J. M. et al. An integrative index of Ecosystem Services provision based on remotely sensed data. *Ecological Indicators* 71, 145–154 (2016). URL <https://www.sciencedirect.com/science/article/pii/S1470160X16303843>. Publisher:Elsevier.
28. Helman, D., Mussery, A., Lensky, I. M. & Leu, S. Detecting changes in biomass productivity in a different land management regimes in drylands using satellite-derived vegetation index. *Soil Use and Management* 30, 32–39 (2014). URL <https://bsssjournals.onlinelibrary.wiley.com/doi/10.1111/sum.12099>.
29. Tollerud, H., Brown, J., Loveland, T., Mahmood, R. & Bliss, N. Drought and Land-Cover Conditions in the Great Plains. *Earth Interactions* 22, 1–25 (2018). URL <https://journals.ametsoc.org/doi/10.1175/EI-D-17-0025.1>.
30. Marumbwa, F. M., Cho, M. A. & Chirwa, P. W. An assessment of remotesensing-based drought index over different land cover types in southern Africa. *International Journal of Remote Sensing* 41, 7368–7382 (2020). URL <https://www.tandfonline.com/doi/full/10.1080/01431161.2020.1757783>.
31. Winkler, K., Fuchs, R., Rounsevell, M. & Herold, M. Global land use changes are four times greater than previously estimated. *Nature Communications* 12, 2501 (2021). URL <https://www.nature.com/articles/s41467-021-22702-2>.
32. Song, X.-P. et al. Global land change from 1982 to 2016. *Nature* 560, 639–643 (2018). URL <https://www.nature.com/articles/s41586-018-0411-9>.
33. Chen, J. et al. Assessing the impact of drought-land cover change on global vegetation greenness and productivity. *Science of The Total Environment* 852, 158499 (2022). URL <https://linkinghub.elsevier.com/retrieve/pii/S004896972205598X>.
34. Akinyemi, F. O. Vegetation Trends, Drought Severity and Land Use-Land Cover Change during the Growing Season in Semi-Arid Contexts. *Remote Sensing* 2021, Vol. 13, Page 836 13, 836 (2021). URL <https://www.mdpi.com/2072-4292/13/5/836/htm>. Publisher: Multidisciplinary Digital Publishing Institute.
35. Peng, D. et al. Country-level net primary production distribution and response to drought and land cover change. *Science of The Total Environment* 574, 65–77(2017). URL <https://linkinghub.elsevier.com/retrieve/pii/S0048969716319507>.
36. Craine, J. M. et al. Global diversity of drought tolerance and grassland climate-change resilience. *Nature Climate Change* 3, 63–67 (2013). URL <https://www.nature.com/articles/nclimate1634>.
37. McDowell, N. G. et al. Mechanisms of woody-plant mortality under rising drought, CO₂ and vapour pressure deficit. *Nature Reviews Earth & Environment* 3, 294–308 (2022). URL <https://www.nature.com/articles/s43017-022-00272-1>.
38. Vicente-Serrano, S. M. et al. Reference evapotranspiration variability and trends in Spain, 1961–2011. *Global and Planetary Change* 121, 26–40 (2014). URL <https://linkinghub.elsevier.com/retrieve/pii/S0921818114001180>.
39. Karabulut, A., Yazıcı Karabulut, B., Demir Yetiş, A., Yeşilnacar, M. & Derin, P. Socioeconomic driving forces of land use/cover changes in the semi-arid Harran plain and their probable implications on arising groundwater level, the GAP area of southeastern Türkiye. *Acta Geophysica* 71, 2795–2810 (2023). URL <https://link.springer.com/10.1007/s11600-023-01162-w>.
40. Beck, H. E. et al. High-resolution (1 km) Köppen-Geiger maps for 1901–2099 based on constrained CMIP6 projections. *Scientific Data* 10 (2023). URL <http://dx.doi.org/10.1038/s41597-023-02549-6>.
41. Luebert, F. & Plischoff, P. The vegetation of Chile and the EcoVeg approach in the context of the International Vegetation Classification project. *Vegetation Classification and Survey* 3, 15–28 (2022). URL <https://vcs.pensoft.net/article/67893/>.
42. Garreaud, R. et al. The 2010–2015 mega drought in Central Chile: Impacts on regional hydroclimate and vegetation. *Hydrology and Earth System Sciences Discussions* 2017, 1–37 (2017). URL <http://www.hydrol-earth-syst-sci-discuss.net/hess-2017-191/>.
43. Miranda, A. et al. Forest browning trends in response to drought in a highly threatened mediterranean landscape of South America. *Ecological Indicators* 115, 106401 (2020). URL <https://linkinghub.elsevier.com/retrieve/pii/S1470160X20303381>.

44. Urrutia-Jalabert, R., González, M. E., González-Reyes, ◆, Lara, A. & Garreaud, R. Climate variability and forest fires in central and south-central Chile. *Ecosphere* 9, e02171 (2018). URL <https://esajournals.onlinelibrary.wiley.com/doi/10.1002/ecs2.2171>.
45. Venegas-González, A., Juñent, F. R., Gutiérrez, A. G. & Filho, M. T. Recent radial growth decline in response to increased drought conditions in the northern most Nothofagus populations from South America. *Forest Ecology and Management* 409, 94–104 (2018). URL <https://linkinghub.elsevier.com/retrieve/pii/S0378112717313993>.
46. Zambrano, F., Lillo-Saavedra, M., Verbist, K. & Lagos, O. Sixteen years of agricultural drought assessment of the biobío region in Chile using a 250 m resolution vegetation condition index (VCI). *Remote Sensing* 8, 1–20 (2016). URL <http://www.mdpi.com/2072-4292/8/6/530>. Publisher: Multidisciplinary Digital Publishing Institute.
47. Zambrano, F., Vrieling, A., Nelson, A., Meroni, M. & Tadesse, T. Prediction of drought-induced reduction of agricultural productivity in Chile from MODIS, rainfall estimates, and climate oscillation indices. *Remote Sensing of Environment* 219, 15–30 (2018). URL <https://www.sciencedirect.com/science/article/pii/S0034425718304541>. Publisher: Elsevier.]
48. Zambrano, F. in *Four decades of satellite data for agricultural drought monitoring throughout the growing season in Central Chile* (eds Vijay P. Singh Deepak Jhajharia, R. M. & Kumar, R.) *Integrated Drought Management, Two Volume Set* 28 (CRC Press, 2023).
49. Aceituno, P., Boisier, J. P., Garreaud, R., Rondanelli, R. & Ruttant, J. A. in *Climate and Weather in Chile* (eds Fernández, B. & Gironás, J.) *Water Resources of Chile, Vol. 8* 7–29 (Springer International Publishing, Cham, 2021).
50. Garreaud, R. D. The Andes climate and weather. *Advances in Geosciences* 22, 3–11 (2009). URL <https://adgeo.copernicus.org/articles/22/3/2009/>.
51. Dinerstein, E. et al. An Ecoregion-Based Approach to Protecting Half the Terrestrial Realm. *BioScience* 67, 534–545 (2017). URL <https://academic.oup.com/bioscience/article-lookup/doi/10.1093/biosci/bix014>.
52. Didan, K. MOD13Q1 MODIS/Terra Vegetation Indices 16-Day L3 Global 250m SIN Grid V006. Tech. Rep., NASA EOSDIS Land Processes DAAC (2015).
53. Running, S., Mu, Q. & Zhao, M. MOD16A2 MODIS/Terra Net Evapotranspiration 8-Day L4 Global 500m SIN Grid V006 (2017). URL <https://lpdaac.usgs.gov/products/mod16a2v006/>.
54. Muñoz-Sabater, J. et al. ERA5-Land: a state-of-the-art global reanalysis dataset for land applications. *Earth System Science Data* 13, 4349–4383 (2021). URL <https://essd.copernicus.org/articles/13/4349/2021/>.
55. Meijer, J. R., Huijbregts, M. A. J., Schotten, K. C. G. J. & Schipper, A. M. Global patterns of current and future road infrastructure. *Environmental Research Letters* 13, 064006 (2018). URL <https://iopscience.iop.org/article/10.1088/1748-9326/aabd42>.
56. Román, M. O. et al. NASA's Black Marble nighttime lights product suite. *Remote Sensing of Environment* 210, 113–143 (2018). URL <https://linkinghub.elsevier.com/retrieve/pii/S003442571830110X>.
57. Halpern, B. S. et al. Spatial and temporal changes in cumulative human impacts on the world's ocean. *Nature Communications* 6, 7615 (2015). URL <https://www.nature.com/articles/ncomms8615>.
58. Halpern, B. S. et al. A Global Map of Human Impact on Marine Ecosystems. *Science* 319, 948–952 (2008). URL <https://www.science.org/doi/10.1126/science.1149345>.
59. Bowler, D. E. et al. Mapping human pressures on biodiversity across the planet uncovers anthropogenic threat complexes. *People and Nature* 2, 380–394 (2020). URL <https://besjournals.onlinelibrary.wiley.com/doi/10.1002/pan3.10071>.
60. Kennedy, C. M., Oakleaf, J. R., Theobald, D. M., Baruch-Mordo, S. & Kiesecker, J. Managing the middle: A shift in conservation priorities based on the global human modification gradient. *Global Change Biology* 25, 811–826 (2019). URL <https://onlinelibrary.wiley.com/doi/10.1111/gcb.14549>.
61. Chen, Q., Timmermans, J., Wen, W. & Van Bodegom, P. M. Ecosystems threatened by intensified drought with divergent vulnerability. *Remote Sensing of Environment* 289, 113512 (2023). URL <https://linkinghub.elsevier.com/retrieve/pii/S0034425723000639>.
62. Hargreaves, G. H. Defining and Using Reference Evapotranspiration. *Journal of Irrigation and Drainage Engineering* 120, 1132–1139 (1994). URL <https://ascelibrary.org/doi/10.1061/%28ASCE%290733-9437%281994%29120%3A6%281132%29>.
63. Hargreaves, G. H. & Samani, Z. A. Reference crop evapotranspiration from temperature. *Applied engineering in agriculture* 1, 96–99 (1985).
64. Heim, R. R. A Review of Twentieth-Century Drought Indices Used in the United States. *Bulletin of the American Meteorological Society* 83, 1149–1166 (2002). URL <https://journals.ametsoc.org/doi/10.1175/1520-0477-83.8.1149>.
65. Laimighofer, J. & Laaha, G. How standard are standardized drought indices? Uncertainty components for the SPI & SPEI case. *Journal of Hydrology* 613, 128385 (2022). URL <https://linkinghub.elsevier.com/retrieve/pii/S0022169422009544>.
66. Farahmand, A. & AghaKouchak, A. A generalized framework for deriving nonparametric standardized drought indicators. *Advances in Water Resources* 76, 140–145 (2015). URL <https://linkinghub.elsevier.com/retrieve/pii/S0309170814002322>.

67. Hobbins, M. T. et al. The Evaporative Demand Drought Index. Part I: Linking Drought Evolution to Variations in Evaporative Demand. *Journal of Hydrometeorology* 17, 1745–1761 (2016). URL <http://journals.ametsoc.org/doi/10.1175/JHM-D-15-0121.1>.
68. Vicente-Serrano, S. M., Beguería, S. & López-Moreno, J. I. A multiscalar drought index sensitive to global warming: The standardized precipitation evapotranspiration index. *Journal of Climate* 23, 1696–1718 (2010). URL <http://dx.doi.org/10.1175/2009JCLI2909.1>.
69. Li, W. et al. Widespread increasing vegetation sensitivity to soil moisture. *Nature Communications* 13, 3959 (2022). URL <https://www.nature.com/articles/s41467-022-31667-9>.
70. Hao, Z. & AghaKouchak, A. Multivariate Standardized Drought Index: A parametric multi-index model. *Advances in Water Resources* 57, 12–18 (2013). URL <https://linkinghub.elsevier.com/retrieve/pii/S0309170813000493>.
71. Wilks, D. S. Empirical distributions and exploratory data analysis. *Statistical Methods in the Atmospheric Sciences* 100 (2011).
72. Abramowitz, M. & Stegun, I. A. *Handbook of mathematical functions with formulas, graphs, and mathematical tables* Vol. 55 (US Government printing office, 1968).
73. Yue, S. & Wang, C. The Mann-Kendall Test Modified by Effective Sample Size to Detect Trend in Serially Correlated Hydrological Series. *Water Resources Management* 18, 201–218 (2004). URL <http://link.springer.com/10.1023/B:WARM.0000043140.61082.60>.
74. Sen, P. K. Estimates of the Regression Coefficient Based on Kendall's Tau. *Journal of the American Statistical Association* 63, 1379–1389 (1968). URL <http://www.tandfonline.com/doi/abs/10.1080/01621459.1968.10480934>.
75. FAO. *The State of the World's Forests 2022* (FAO, 2022). URL <http://www.fao.org/documents/card/en/c/cb9360en>.
76. Zhao, Y. et al. Detailed dynamic land cover mapping of Chile: Accuracy improvement by integrating multi-temporal data. *Remote Sensing of Environment* 183, 170–185 (2016). URL <https://linkinghub.elsevier.com/retrieve/pii/S0034425716302188>.
77. Dormann, C. F. et al. Collinearity: a review of methods to deal with it and a simulation study evaluating their performance. *Ecography* 36, 27–46 (2013). URL <https://onlinelibrary.wiley.com/doi/10.1111/j.1600-0587.2012.07348.x>.
78. R Core Team. *R: A Language and Environment for Statistical Computing* (R Foundation for Statistical Computing, Vienna, Austria, 2023). URL <https://www.R-project.org/>.
79. Hufkens, K., Stauffer, R. & Campitelli, E. The *ecwmfr* package: an interface to ECMWF API endpoints (2019). URL <https://bluegreen-labs.github.io/ecwmfr/>.
80. Hijmans, R. J. *terra: Spatial Data Analysis* (2023). URL <https://CRAN.R-project.org/package=terra>.
81. Pebesma, E. & Bivand, R. *Spatial Data Science: With applications in R* (Chapman and Hall/CRC, London, 2023). URL <https://r-spatial.org/book/>.
82. Pebesma, E. Simple Features for R: Standardized Support for Spatial Vector Data. *The R Journal* 10, 439–446 (2018). URL <https://doi.org/10.32614/RJ-2018-009>.
83. Beguería, S. & Vicente-Serrano, S. M. *SPEI: Calculation of the Standardized Precipitation-Evapotranspiration Index* (2023). URL <https://CRAN.R-project.org/package=SPEI>.
84. Tennekes, M. *tmap: Thematic Maps in R*. *Journal of Statistical Software* 84, 1–39 (2018).
85. Wickham, H. et al. Welcome to the tidyverse. *Journal of Open Source Software* 4, 1686 (2019).
86. Kuhn, M. & Wickham, H. *Tidymodels: a collection of packages for modeling and machine learning using tidyverse principles*. (2020). URL <https://www.tidymodels.org>.
87. Wright, M. N. & Ziegler, A. *ranger: A Fast Implementation of Random Forests for High Dimensional Data in C++ and R*. *Journal of Statistical Software* 77, 1–17 (2017).
88. Boisier, J. P. et al. Anthropogenic drying in central-southern Chile evidenced by long-term observations and climate model simulations. *Elementa* 6, 74 (2018). URL <https://www.elementascience.org/article/10.1525/elementa.328/>.
89. Sarricolea, P., Meseguer-Ruiz, Serrano-Notivol, R., Soto, M. V. & Martín-Vide, J. Trends of daily precipitation concentration in Central-Southern Chile. *Atmospheric Research* 215, 85–98 (2019). URL <https://linkinghub.elsevier.com/retrieve/pii/S0169809518308512>.
90. Rashid, M. M. & Beecham, S. Characterization of meteorological droughts across South Australia. *Meteorological Applications* 26, 556–568 (2019). URL <https://rmets.onlinelibrary.wiley.com/doi/10.1002/met.1783>.
91. Miró, J. J., Estrela, M. J., Corell, D., Gómez, I. & Luna, M. Y. Precipitation and drought trends (1952–2021) in a key hydrological recharge area of the eastern Iberian Peninsula. *Atmospheric Research* 286, 106695 (2023). URL <https://linkinghub.elsevier.com/retrieve/pii/S0169809523000923>.
92. Páscoa, P. et al. A high-resolution view of the recent drought trends over the Iberian Peninsula. *Weather and Climate Extremes* 32, 100320 (2021). URL <https://linkinghub.elsevier.com/retrieve/pii/S2212094721000189>.
93. Taucare, M., Viguier, B., Figueroa, R. & Daniele, L. The alarming state of Central Chile's groundwater resources: A paradigmatic case of a lasting over-exploitation. *Science of The Total Environment* 906, 167723 (2024). URL <https://linkinghub.elsevier.com/retrieve/pii/S0048969723063507>.
94. Nicolai-Shaw, N., Zscheischler, J., Hirschi, M., Gudmundsson, L. & Seneviratne, S. I. A drought event composite analysis using satellite remote-sensing based soil moisture. *Remote Sensing of Environment* 203, 216–225 (2017). URL <https://linkinghub.elsevier.com/retrieve/pii/S0034425717302729>.

95. Jiang, W., Wang, L., Feng, L., Zhang, M. & Yao, R. Drought characteristics and its impact on changes in surface vegetation from 1981 to 2015 in the Yangtze River Basin, China. *International Journal of Climatology* 40, 3380–3397 (2020). URL <https://rmets.onlinelibrary.wiley.com/doi/10.1002/joc.6403>.
96. Zhou, K., Li, J., Zhang, T. & Kang, A. The use of combined soil moisture data to characterize agricultural drought conditions and the relationship among different drought types in China. *Agricultural Water Management* 243, 106479 (2021). URL <https://linkinghub.elsevier.com/retrieve/pii/S0378377420305965>.
97. Venegas-González, A. et al. Sclerophyllous Forest Tree Growth Under the Influence of a Historic Megadrought in the Mediterranean Ecoregion of Chile. *Ecosystems* 26, 344–361 (2023). URL <https://link.springer.com/10.1007/s10021-022-00760-x>.
98. Carrasco, G. et al. Effects of climate change on forest plantation productivity in Chile. *Global Change Biology* 28, 7391–7409 (2022). URL <https://onlinelibrary.wiley.com/doi/10.1111/gcb.16418>.
99. Fajardo, A., Gazol, A., Mayr, C. & Camarero, J. J. Recent decadal drought reverts warming-triggered growth enhancement in contrasting climates in the southern Andes tree line. *Journal of Biogeography* 46, 1367–1379 (2019). URL <https://onlinelibrary.wiley.com/doi/10.1111/jbi.13580>.
100. Holz, A., Hart, S. J., Williamson, G. J., Veblen, T. T. & Aravena, J. C. Radial growth response to climate change along the latitudinal range of the world's southernmost conifer in southern South America. *Journal of Biogeography* 45, 1140–1152 (2018). URL <https://onlinelibrary.wiley.com/doi/10.1111/jbi.13199>.
101. Segovia, R. A. et al. Freezing and water availability structure the evolutionary diversity of trees across the Americas. *Science Advances* 6, eaaz5373 (2020). URL <https://www.science.org/doi/10.1126/sciadv.aaz5373>.
102. Sabatini, F. M. et al. Global patterns of vascular plant alpha diversity. *Nature Communications* 13, 4683 (2022). URL <https://www.nature.com/articles/s41467-022-32063-z>.
103. Holden, Z. A. et al. Decreasing fire season precipitation increased recent western US forest wildfire activity. *Proceedings of the National Academy of Sciences* 115 (2018). URL <https://pnas.org/doi/full/10.1073/pnas.1802316115>.
104. González, M. E., Gómez-González, S., Lara, A., Garreaud, R. & Díaz-Hormazábal, I. The 2010–2015 Megadrought and its influence on the fire regime in central and south-central Chile. *Ecosphere* 9, e02300 (2018). URL <https://esajournals.onlinelibrary.wiley.com/doi/10.1002/ecs2.2300>.
105. Bowman, D. M. J. S. et al. Human–environmental drivers and impacts of the globally extreme 2017 Chilean fires. *Ambio* 48, 350–362 (2019). URL <http://link.springer.com/10.1007/s13280-018-1084-1>.
106. Quiring, S. M. & Ganesh, S. Evaluating the utility of the Vegetation Condition Index (VCI) for monitoring meteorological drought in Texas. *Agricultural and Forest Meteorology* 150, 330–339 (2010). URL <http://www.sciencedirect.com/science/article/pii/S0168192309002809>.
107. Muñoz, A. A. et al. Water Crisis in Petorca Basin, Chile: The Combined Effects of a Mega-Drought and Water Management. *Water* 12, 648 (2020). URL <https://www.mdpi.com/2073-4441/12/3/648>.
108. Duran-Llacer, I. et al. Lessons to Be Learned: Groundwater Depletion in Chile's Ligua and Petorca Watersheds through an Interdisciplinary Approach. *Water* 12, 2446 (2020). URL <https://www.mdpi.com/2073-4441/12/9/2446>.
109. Hermans, K. & McLeman, R. Climate change, drought, land degradation and migration: exploring the linkages. *Current Opinion in Environmental Sustainability* 50, 236–244 (2021). URL <https://linkinghub.elsevier.com/retrieve/pii/S1877343521000701>.
110. Smith-Ramírez, C. et al. Combining remote sensing and field data to assess recovery of the Chilean Mediterranean vegetation after fire: Effect of time elapsed and burn severity. *Forest Ecology and Management* 503, 119800 (2022). URL <https://linkinghub.elsevier.com/retrieve/pii/S0378112721008914>.
111. Gomis-Cebolla, J., Rattayova, V., Salazar-Galán, S. & Francés, F. Evaluation of ERA5 and ERA5-Land reanalysis precipitation datasets over Spain (1951–2020). *Atmospheric Research* 284, 106606 (2023). URL <https://linkinghub.elsevier.com/retrieve/pii/S0169809523000030>.
112. Clelland, A. A., Marshall, G. J. & Baxter, R. Evaluating the performance of key ERA-Interim , ERA5 and ERA5-Land climate variables across Siberia. *International Journal of Climatology* 44, 2318–2342 (2024). URL <https://rmets.onlinelibrary.wiley.com/doi/10.1002/joc.8456>.
113. Stehman, S. V. & Foody, G. M. Key issues in rigorous accuracy assessment of land cover products. *Remote Sensing of Environment* 231, 111199 (2019). URL <https://linkinghub.elsevier.com/retrieve/pii/S0034425719302111>.
114. Verburg, P. H., Neumann, K. & Nol, L. Challenges in using land use and land cover data for global change studies. *Global Change Biology* 17, 974–989 (2011). URL <https://onlinelibrary.wiley.com/doi/10.1111/j.1365-2486.2010.02307.x>.
115. Rindfuss, R. R., Walsh, S. J., Turner, B. L., Fox, J. & Mishra, V. Developing a science of land change: Challenges and methodological issues. *Proceedings of the National Academy of Sciences* 101, 13976–13981 (2004). URL <https://pnas.org/doi/full/10.1073/pnas.0401545101>.
116. Jenner, L., Metzger, M., Moseley, D., Peskett, L. & Forrest, E. The limitations and risks of land use change tools in decision-making: Lessons from Galloway and Southern Ayrshire UNESCO Biosphere, Scotland. *Environmental Science & Policy* 161, 103889 (2024). URL <https://linkinghub.elsevier.com/retrieve/pii/S1462901124002235>.